Stability of Brillouin flow in planar, conventional, and inverted magnetrons

D. H. Simon,[1] Y. Y. Lau,[1] G. Greening,[1] P. Wong,[1] B. W. Hoff,[2] and R. M. Gilgenbach[1]
[1]*Department of Nuclear Engineering and Radiological Sciences, University of Michigan, Ann Arbor, Michigan 48109-2104, USA*
[2]*Air Force Research Laboratory, Kirtland Air Force Base, Albuquerque, New Mexico 87117, USA*

(Received 21 May 2015; accepted 13 July 2015; published online 4 August 2015)

The Brillouin flow is the prevalent flow in crossed-field devices. We systematically study its stability in the conventional, planar, and inverted magnetron geometry. To investigate the intrinsic negative mass effect in Brillouin flow, we consider electrostatic modes in a nonrelativistic, smooth bore magnetron. We found that the Brillouin flow in the inverted magnetron is more unstable than that in a planar magnetron, which in turn is more unstable than that in the conventional magnetron. Thus, oscillations in the inverted magnetron may startup faster than the conventional magnetron. This result is consistent with simulations, and with the negative mass property in the inverted magnetron configuration. Inclusion of relativistic effects and electromagnetic effects does not qualitatively change these conclusions. © *2015 AIP Publishing LLC*.
[http://dx.doi.org/10.1063/1.4927798]

I. INTRODUCTION

The inverted magnetron is a crossed-field device with the cathode on the outside instead of the inside, as is the case in conventional magnetrons. It continues to spark interest, as it has some marked advantages over a conventional magnetron. The larger cathode area allows for more current, and the centripetal force on the electrons acts in the same direction as the magnetic force, which reduces the magnetic field required for insulation of the anode. Simulations of the recirculating planar magnetron (RPM)[1–3] show that bunching occurred in the recirculating bends if the device was in an inverted configuration.

In the inverted magnetron configuration, a rotating electron possesses a "negative mass" effect, so that a *thin* axis-encircling electron layer is subject to the negative mass instability.[4,5] In such a thin electron layer, the negative mass instability is the dominant instability, and the diocotron instability is the residual instability which becomes dominant in the planar limit, in which case the negative mass effect is absent.[4] Unanswered is the negative mass effect in a rotating Brillouin flow, whose electron hub is not "thin." Moreover, the very significant velocity shear in the Brillouin flow intrinsically represents a large velocity spread, which tends to stabilize the negative mass instability on a thin electron beam. Since the Brillouin flow is the prevalent state in a crossed-field geometry,[6,7] we systematically study its stability in conventional, planar, and inverted magnetron configurations. To investigate the intrinsic negative mass effects in Brillouin flows, we consider electrostatic modes in a nonrelativistic, smooth bore magnetron.

The negative mass instability is a cylindrical effect. For a *thin* rotating electron beam, it is characterized by the dimensionless parameter $h = eE_0r/\gamma_0^3mc^2\beta_0^2$ which is a measure of the ratio of the electric force to centripetal force.[4,8] Here, e is the magnitude of the charge of an electron, m is the rest mass of an electron, E is the electric field at the electron beam, r is the radius of the electron beam, β_0 is the azimuthal velocity of the beam divided by the speed of light, c, and $\gamma = 1/\sqrt{1-\beta_0^2}$ is the relativistic mass factor. Negative mass instability on a thin electron beam occurs when $h > -\beta_0^2/2$.[4,5,8] For electrons, this condition will always be satisfied if the radial electric field E_0 is positive, as in an inverted magnetron configuration. An electron in the conventional magnetron configuration would exhibit a positive mass behavior. Since Brillouin flow has a substantial thickness and has very significant velocity shear within the flow as indicated above, it is unclear if the notion of negative mass instability applies. It should be stressed that the Brillouin flow, because of its strong velocity shear, is subjected to a diocotron-like instability. The stability of Brillouin flow in the planar magnetron and the conventional magnetron configuration has been studied extensively by Buneman,[9] Swegle,[10] Antonsen,[11] Davidson,[12,13] and Tsang.[14] The geometries they consider exclude negative mass behavior. They include only positive mass behavior.

In order to isolate the effects of the negative mass instability from the velocity shear which is always present in the Brillouin flow, the planar case is briefly revisited first. A comparison between the growth rates of planar, conventional, and inverted magnetrons in the non-relativistic regime then illustrates the positive or negative mass effects on the shear flow instability. We show that the inverted magnetron has a higher instability growth rate than the planar magnetron, while the conventional magnetron has the lowest growth rate.

In Section II, we summarize the results for the stability of the planar Brillouin flow. In Section III, we compare the Brillouin flow stability in the planar, conventional, and inverted magnetron configurations. We also consider the azimuthal modes that would sequentially be excited as the gap voltage is ramped up. In Section III, we include the results on relativistic and electromagnetic effects (still for the smooth bore configuration). Concluding remarks are given in Section IV.

 © 2015 AIP Publishing LLC

II. STABILITY OF PLANAR BRILLOUIN FLOW

The planar Brillouin flow geometry is shown in Fig. 1. In equilibrium, a voltage V is imposed across the anode-cathode (AK) gap with gap separation D. The Brillouin flow is a cold, laminar shear flow in the y-direction with linear velocity $\mathbf{v_0} = \mathbf{y}\omega_c x$, which increases linearly from the cathode ($x = 0$) to the top of the Brillouin hub ($x = d$). Here, $\omega_c = eB_0/m$, where B_0 is the equilibrium magnetic field in the z-direction (Fig. 1). The Brillouin flow has constant electron density n_0 within the Brillouin hub ($0 < x < d$) with the property $\omega_p^2 = \omega_c^2$, where $\omega_p^2 = e^2 n_0/m\varepsilon_0$. In terms of V, B_0, and D, the Brillouin hub height is given by $d = D(1 - \sqrt{1 - V/V_H})$, where $V_H = (1/2)(m/e)(\omega_c D)^2$ is the Hartree voltage. See, e.g., Ref. 8. The vacuum region has a width $W = D - d$ (Fig. 1).

The stability of planar Brillouin flow under is well documented.[9–14] For perturbation quantities with $\exp(i\omega t - ik_y y)$ dependence, the principal equations are presented here in dimensionless form using the following variables:

$$\bar{x} = xk_y, \quad \bar{\omega} = \frac{\omega}{|\omega_c|} \equiv \bar{\omega}_r - i\bar{\omega}_i, \quad \bar{\Omega} = \bar{\omega} - \bar{x}, \qquad (1)$$

so that $\bar{\omega}_i$ is the normalized growth rate. The governing equation reads

$$\frac{\partial^2 \phi_1}{\partial \bar{x}^2} = \phi_1 + \frac{2}{\bar{\Omega}^3 - \bar{\Omega}}\left(\frac{\partial \phi_1}{\partial \bar{x}} + \frac{\phi_1}{\bar{\Omega}}\right). \qquad (2)$$

The vacuum boundary condition is

$$\left.\frac{1}{\phi_1}\frac{\partial \phi_1}{\partial \bar{x}}\right|_{r_{vac}} = -\coth(\bar{W}), \qquad (3)$$

and the jump condition reads

$$\left.\frac{1}{\phi_1}\frac{\partial \phi_1}{\partial \bar{x}}\right|_{r_{vac}} = \left.\frac{1}{\phi_1}\frac{\partial \phi_1}{\partial \bar{x}}\right|_{r_{hub}} - \left.\frac{1}{\bar{\Omega}^2}\left(\frac{1}{\phi_1}\frac{\partial \phi_1}{\partial \bar{x}} + \frac{1}{\bar{\Omega}}\right)\right|_{r_{hub}}. \qquad (4)$$

The solution to the above set of equations is shown in Fig. 2 for different wave numbers (through $\bar{d} = k_y d$) for the case where $\bar{d} = \bar{W}$. This case of 50% fill represents intermediate magnetic insulation and is also common for relativistic magnetrons. The distance between the hub and the anode, $\bar{W}$, enters only in the vacuum boundary condition as $\coth(\bar{W})$ which is roughly a constant (=1) over the entire range of $\bar{W}$. The real part of the frequency increases linearly with k_y (i.e., with $\bar{d}$). We found that, for large values of $\bar{d}$, $\bar{d} - \bar{\omega}_r = 0.55$ and $\bar{\omega}_i = 0.06$, a result proven by Buneman, Levy, and Linson.[9] The real part of the frequency corresponds to a synchronous layer within the Brillouin hub. The system is stable below a certain threshold, namely, there is no instability if the real part of the frequency is less than the electron cyclotron frequency.[10]

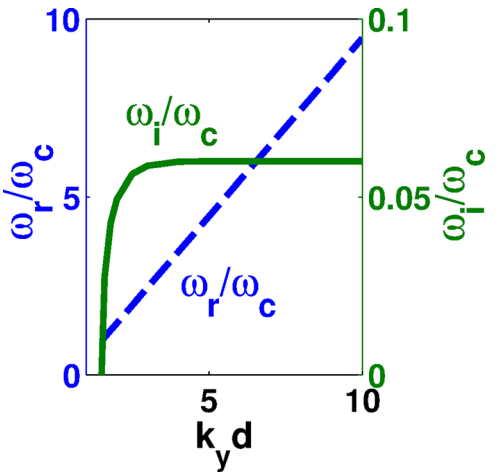

FIG. 2. Planar magnetron eigenvalue solutions for the case where $\bar{d} = \bar{W}$. This condition completely defines the normalized variables in the eigenvalue problem.

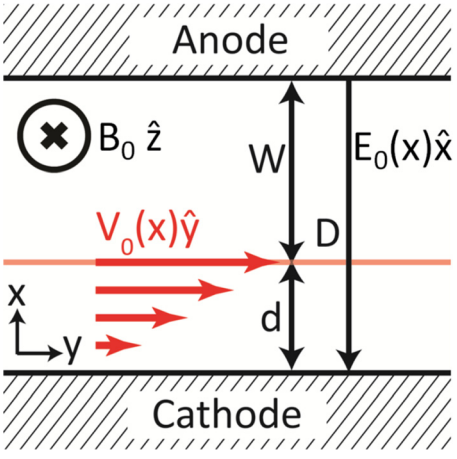

FIG. 1. Planar Brillouin flow.

III. STABILITY OF CYLINDRICAL BRILLOUIN FLOW IN CONVENTIONAL AND INVERTED MAGNETRON

We use r_a, r_b, and r_c to designate, respectively, the anode radius, the Brillouin hub radius, and the cathode radius in both conventional magnetron and inverted magnetron configurations. Figure 3 shows the inverted geometry. Cylindrical Brillouin flow, like the planar version, has the property

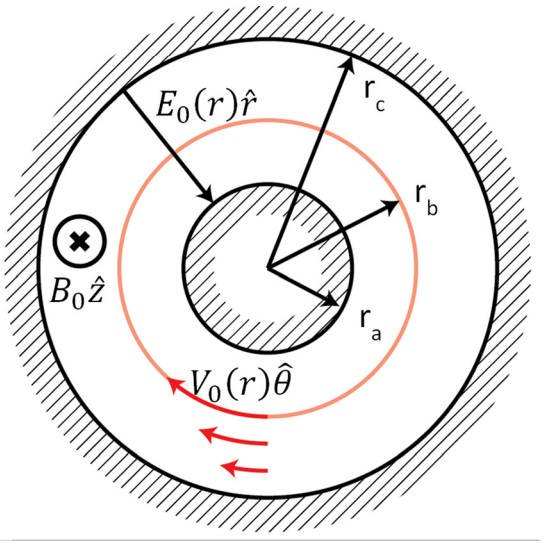

FIG. 3. Brillouin flow in the inverted magnetron configuration.

$\omega_p^2 = \omega_c^2$ at the cathode, though since the density varies radially, this does not hold true for the rest of the Brillouin hub. The following dimensionless equations are applicable to both the normal and inverted magnetron configurations, where $+\bar{\omega}$ $(-\bar{\omega})$ is used in the equation for $\bar{\Omega}$ in the conventional (inverted) magnetron configuration, and ℓ $(\ell > 0)$ is the azimuthal mode number:

$$\bar{r} = \frac{r}{r_c}, \quad \bar{\omega} = \frac{\omega}{|\omega_c|} = \bar{\omega}_r - i\bar{\omega}_i,$$
$$\bar{\Omega} = \pm\bar{\omega} - \frac{1}{2}l\left(1 - \frac{1}{\bar{r}^2}\right), \quad \bar{\omega}_p^2 = \frac{1}{2}\left(1 + \frac{1}{\bar{r}^4}\right). \tag{5}$$

The governing equation reads

$$\phi_1'' = \frac{l^2}{\bar{r}^2}\phi_1 - \frac{\phi_1'}{\bar{r}} + \frac{2l\bar{\omega}_p^2}{\bar{\Omega}\left(\bar{\Omega}^2 - \bar{\omega}_p^2\right)}\left[\frac{\phi_1'}{\bar{r}^3} + \left(\frac{l}{\bar{r}^6\bar{\Omega}} - \frac{1}{\bar{r}^4}\right)\phi_1\right]$$
$$- \frac{2}{\left(\bar{\Omega}^2 - \bar{\omega}_p^2\right)}\left(\frac{\phi_1'}{\bar{r}^5} + \frac{l\phi_1}{\bar{r}^8\bar{\Omega}}\right). \tag{6}$$

The boundary condition in the vacuum region outside the Brillouin hub is

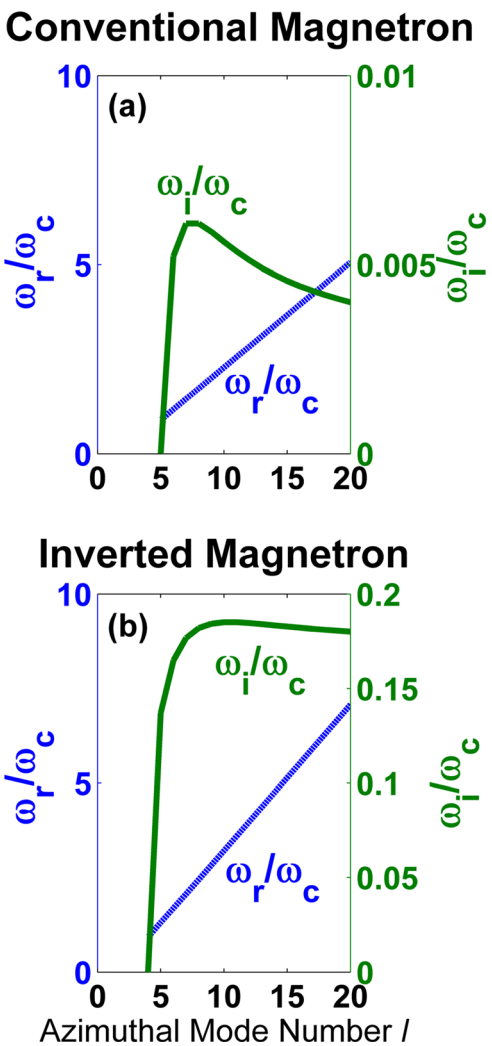

FIG. 4. The eigenvalue solutions for the conventional (a) and inverted (b) magnetrons. The inner radius is 1 m, the Brillouin hub radius is 1.5 m, and the outer radius is 2 m.

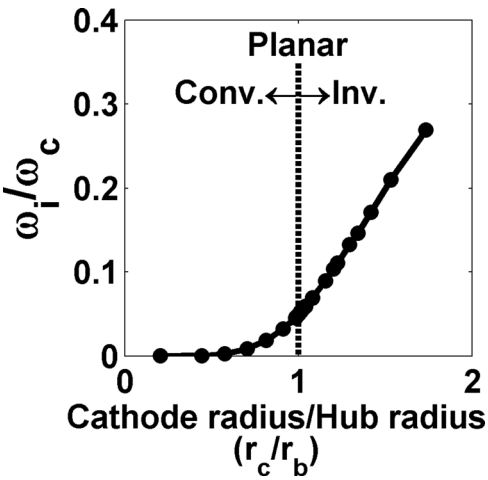

FIG. 5. Normalized growth rate as a function of cathode radius to hub height for a constant AK gap width, hub height, and bunch frequency. The conventional, planar, and inverted magnetrons correspond to, respectively, $r_c/r_b < 1$, $r_c/r_b = 1$, and $r_c/r_b > 1$.

$$\left.\frac{\phi_1'}{\phi_1}\right|_{r_{vac}} = \frac{l}{\bar{r}}\frac{\left[\frac{\overline{r_b}^l}{\overline{r_a}^l} + \frac{\overline{r_a}^l}{\overline{r_b}^l}\right]}{\left[\frac{\overline{r_b}^l}{\overline{r_a}^l} - \frac{\overline{r_a}^l}{\overline{r_b}^l}\right]}, \tag{7}$$

and the jump condition is

$$\left.\frac{\phi_1'}{\phi_1}\right|_{r_{vac}} = \left.\frac{\phi_1'}{\phi_1}\right|_{r_{hub}} - \frac{\bar{\omega}_p^2}{\bar{\Omega}^2}\left.\left(\frac{\phi_1'}{\phi_1} + \frac{l}{\bar{r}^3\bar{\Omega}}\right)\right|_{r_{hub}}. \tag{8}$$

The real part of the frequency shown in Fig. 4 for both conventional and inverted magnetron scales roughly linearly with the mode number (ℓ), as was the case for the planar magnetron. Additionally, the threshold for system stability also occurs at about the point the real frequency is equal to the cyclotron frequency. The imaginary part of the frequency shows a similar trend to the planar system, except that it decreases after reaching a peak instead of approaching an asymptote. Note the large contrast in the growth rate between the conventional magnetron (Fig. 4(a)) and the inverted magnetron (Fig. 4(b)) in this example. We will further explore this contrast in Fig. 5.

The values in Fig. 5 are found from solving the eigenvalue equation for the planar and cylindrical governing equations at different cathode to anode radii ratios. The planar geometry is the limit where cathode radius and anode radius go to infinity, so the ratio is 1. The AK gap separation is held at a constant of 1 m, the Brillouin hub is at a constant 50% fill (0.5 m from the anode and cathode), and the bunch frequency at the top of the hub (lv_0/r_b for cylindrical and $k_y v_0$ for planar, where v_0 is the velocity of electrons at the top of the Brillouin hub) is held constant at $2 \times \omega_c$ while the anode and cathode radii are varied.

The inverted geometry shows an increase in instability strength as the ratio of r_c/r_b increases, starting from the planar ratio of 1. The conventional geometry stabilizes as r_c/r_b decreases from the planar ratio of 1 (Fig. 5). The increase in

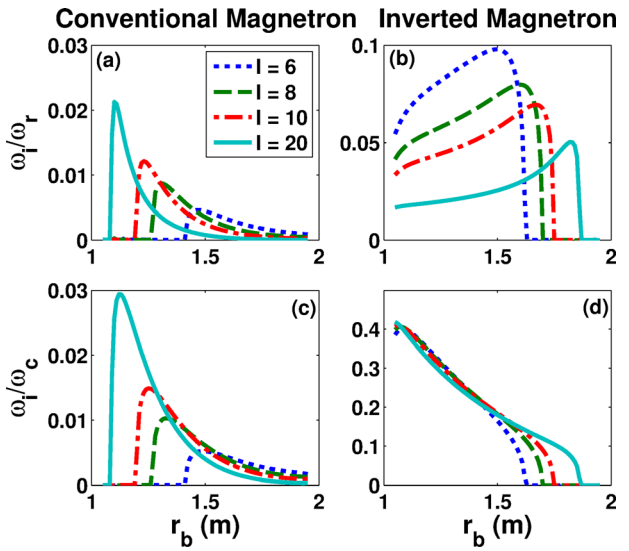

FIG. 6. The ratio of ω_i/ω_r as a function of r_b for a conventional (a) and inverted (b) magnetrons. The ratio of ω_i/ω_c as a function of r_b for a conventional (c) and inverted (d) magnetrons. In all cases, the inner and outer radii are held constant at 1 m and 2 m, respectively. r_b increases as the gap voltage increases for (a) and (c), and decreases for (b) and (d).

r_c/r_b for the inverted geometry and decrease in r_c/r_b for the conventional geometry both correspond to a decrease in inner and outer radii for the magnetrons. This indicates that the inverted magnetron configuration destabilizes the intrinsic instability in the planar system, while the conventional magnetron configuration stabilizes it.

Having shown that the inverted magnetron is inherently more unstable than conventional magnetron, we now explore which modes start up first as the AK gap voltage of the magnetron is turned on, while the magnetic field remains constant. The turn-on is assumed to be sufficiently slow such that the system is in a quasi-static equilibrium. As the voltage is ramped up, the Brillouin hub radius r_b increases in the conventional magnetron shown in Figs. 6(a) and 6(c), but decreases in the inverted magnetron configuration shown in Figs. 6(b) and 6(d). The growth rate is normalized to the real part of the mode frequency in Figs. 6(a) and 6(b) and to the electron cyclotron frequency in Figs. 6(c) and 6(d). In the conventional magnetrons in Figs. 6(a) and 6(c), the higher order modes start up first, and with a higher growth rate than lower order modes. All of the modes lose strength rapidly as the Brillouin hub increases. For the inverted magnetrons in Figs. 6(b) and 6(d), the higher order modes also start up sooner than lower order modes, but they are weaker in that ω_i/ω_r is lower for high ℓ. Additionally, all of the modes show an increase in $\bar{\omega}_i$ as the Brillouin hub increases.

IV. ELECTROMAGNETIC AND RELATIVISTIC EFFECTS

Including relativistic effects in a fully electromagnetic formulation, the perturbed fields are governed by the differential equation, Eq. (14) of Chernin and Lau,[4] with the equilibrium profiles for n(r), v(r), E(r), and B(r) provided by the electromagnetic Brillouin hub equilibrium solution.[13,15] The electromagnetic eigenvalue solutions are found from matching the perturbed azimuthal electric fields in the vacuum

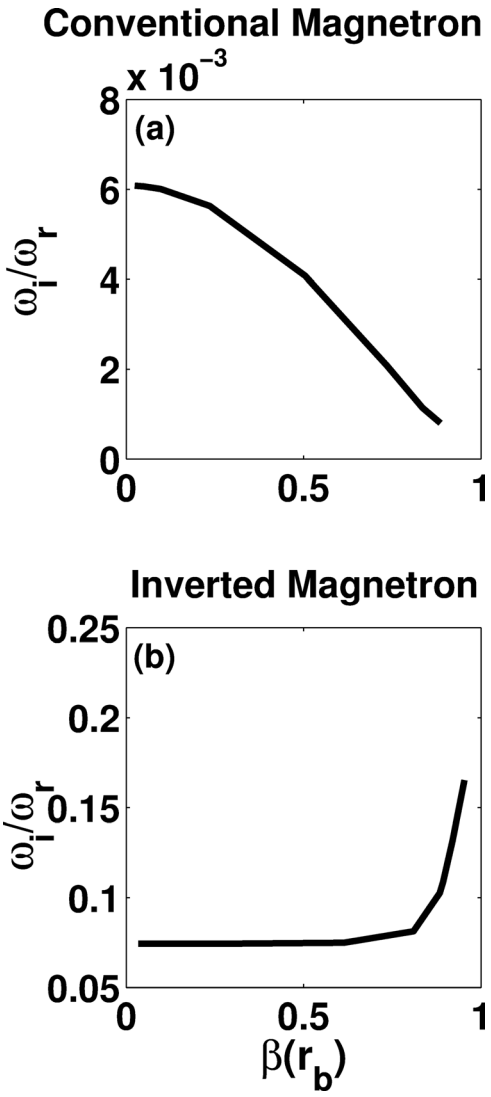

FIG. 7. Normalized growth rate as a function of electron velocity (normalized to the speed of light) at the hub for a conventional (a) and inverted (b) magnetrons. The geometry (1 m inner radius and 2 m outer radius) is held constant, the mode number *l* is set to 8, and the voltage and magnetic field are increased proportionally to achieve a constant hub radius of 1.5 m while increasing the electron velocity at the hub.

region to those in the Brillouin hub. It has been shown that increasing the particle velocity into the relativistic range reduces the normalized instability growth rate for planar geometries.[10]

Figure 7 shows the normalized growth rate for a cylindrical case as the particle's kinetic energy at the hub increases. The configuration used in both figures is a 1 m inner radius, 2 m outer radius, 50% Brillouin hub fill of the AK gap, and a mode number $\ell = 8$. These two figures show that conventional magnetrons experience a decrease in growth rate as electrons become more relativistic, while inverted magnetrons have increased growth in the same situation. As with the aspect ratio studies in Sec. III, it appears that relativistic effect in the inverted magnetron configuration leads to further destabilization, while the conventional magnetron configuration is stabilized.

The inverted configuration in Fig. 7(b) has a fairly flat normalized growth rate until it experiences a rapid increase

at $\beta(r_b)$ greater than about 0.8. This is the region in which the increase in ω_r starts to diminish with the increase in electron energy, and ω_r approaches a limit when the synchronous electrons are reaching the speed of light (since $\omega_r < lv(r_b)/r_b$ for synchronism between the wave and the electrons within the Brillouin hub, and the maximum velocity of $v(r_b)$ is c). The increase in ω_i with electron energy slows down in this region as well, but does not approach a limit. The spike in ω_i/ω_r is caused by this behavior, where ω_i increases with increasing electron energy, but ω_r is limited by the electron velocity. This implies that the instability in the inverted configuration can still exist even as the relativistic mass of the electrons increases greatly.

The conventional magnetron's growth rate [Fig. 7(a)], by contrast, starts to decrease almost immediately with relativistic effects. This difference in behavior is at least partially due to a difference in the behavior of ω_r. In the conventional configuration, the upper limit for electron velocities in the hub is c; however, the synchronous electrons have a velocity limit that is a fraction of c. So the synchronous layer is pushed toward the cathode surface as $v(r_b)$ approaches c (in contrast, in the inverted magnetron, the synchronous layer is pushed toward the Brillouin hub radius r_b as $v(r_b)$ approaches c). The proximity of this synchronous layer and the cathode tends to short out the tangential RF electric field at the synchronous layer, thereby reducing the normalized growth rate in the case of conventional magnetron [Fig. 7(a)].

V. SUMMARY

Dimensionless equations are presented for electrostatic Brillouin flow, in both planar and cylindrical magnetrons. The electrostatic eigenvalue solutions for these equations show that the shear flow instability in the planar geometry is reduced in the conventional cylindrical configuration, but enhanced in the inverted configuration. The amount of reduction or enhancement increases as the radii in the system decrease. This correlation is consistent with the negative mass instability, which is a cylindrical effect based on the ratio of electric force to centripetal force.

The electrostatic startup condition with constant magnetic field is compared between conventional and inverted magnetrons. Both geometries show that the higher order modes start up first as the voltage is ramped up. In the conventional case, the growth rate for any given mode peaks soon after it starts, and then decreases rapidly. On an absolute time scale (normalized to ω_c, Fig. 6(c)), the instability strength of each mode is only slightly different than its nearest neighbors and it decreases as hub height increases. Modes in the inverted case also increase rapidly after starting, but show a very slow decrease in normalized growth rate ω_i/ω_r. This translates into an almost linear increase in ω_i/ω_c with hub height. All modes that enter this regime have roughly equal growth rates, with lower order modes being slightly favored.

The electrostatic results are transitioned smoothly into the electromagnetic regime. The normalized growth rate of the conventional configuration decreases as the electrons at the hub increase in relativistic energy. The inverted case increases as the kinetic energy in the outer hub electrons increases. The planar case shows a decrease in growth rate with an increase in hub electron kinetic energy.

The shear flow instability, or the diocotron-like instability, in a crossed-field geometry has long been conjectured to cause the startup of a magnetron. Here, we showed that the Brillouin flow in the inverted magnetron is intrinsically more unstable than the Brillouin flow in the conventional magnetron, consistent with the simulation results of the recirculating planar magnetron.

ACKNOWLEDGMENTS

This work was supported by Air Force Office of Scientific Research Award Nos. FA9550-10-1-0104 and FA9550-15-1-0097, Office of Naval Research Award No. N00014-13-1-0566, and L-3 Communications Electron Device Division.

[1]R. M. Gilgenbach, Y. Y. Lau, D. M. French, B. W. Hoff, J. Luginsland, and M. Franzi, "Crossed field device," U.S. patent No. US8,841,867 B2 (23 September 2014).
[2]R. M. Gilgenbach, Y.-Y. Lau, D. M. French, B. W. Hoff, M. Franzi, and J. Luginsland, "Recirculating planar magnetrons for high-power high-frequency radiation generation," IEEE Trans. Plasma Sci. **39**(4), 980–987 (2011).
[3]M. A. Franzi, R. M. Gilgenbach, B. W. Hoff, D. A. Chalenski, D. Simon, Y. Y. Lau, and J. Luginsland, "Recirculating-planar-magnetron simulations and experiment," IEEE Trans. Plasma Sci. **41**(4), 639–645 (2013).
[4]D. Chernin and Y. Y. Lau, "Stability of laminar electron layers," Phys. Fluids **27**(9), 2319–2331 (1984).
[5]D. M. French, B. W. Hoff, Y. Y. Lau, and R. M. Gilgenbach, "Negative, positive, and infinite mass properties of a rotating electron beam," Appl. Phys. Lett. **97**(11), 111501 (2010).
[6]J. C. Slater, *Microwave Electronics* (Van Nostrand, New York, 1951), p. 302.
[7]P. J. Christenson, D. P. Chernin, A. L. Garner, and Y. Y. Lau, "Resistive destabilization of cycloidal electron flow and universality of (near-) Brillouin flow in a crossed-field gap," Phys. Plasmas **3**(12), 4455–4462 (1996).
[8]Y. Y. Lau, in *High-Power Microwave Sources*, edited by V. L. Granatstein and I. Alexeff (Artech House, Norwood, MA, 1987), p. 309.
[9]O. Buneman, R. Levy, and L. Linson, "Stability of crossed-field electron beams," J. Appl. Phys. **37**(8), 3203 (1966).
[10]J. Swegle and E. Ott, "Instability of the Brillouin-flow equilibrium in magnetically insulated structures," Phys. Rev. Lett. **46**(14), 929–932 (1981).
[11]T. M. Antonsen, Jr., E. Ott, C. L. Chang, and A. T. Drobot, "Parametric scaling of the stability of relativistic laminar flow magnetic insulation," Phys. Fluids **28**(9), 2878–2881 (1985).
[12]R. Davidson, H.-W. Chan, C. Chen, and S. Lund, "Equilibrium and stability properties of intense non-neutral electron flow," Rev. Mod. Phys. **63**(2), 341–374 (1991).
[13]R. C. Davidson, *Physics of Nonneutral Plasmas* (Imperial College Press, 2001).
[14]K. T. Tsang and R. C. Davidson, "Macroscopic cold-fluid equilibrium properties of relativistic non-neutral electron flow in a cylindrical diode," Phys. Rev. A **33**(6), 4284–4292 (1986).
[15]D. H. Simon, Y. Y. Lau, J. W. Luginsland, and R. M. Gilgenbach, "An unnoticed property of the cylindrical relativistic Brillouin flow," Phys. Plasmas **19**(4), 043103 (2012).